 Acta Chir Orthop Traumatol Cech. 88, 2021, No. 4
p. 313–320

ORIGINAL PAPER
PŮVODNÍ PRÁCE

The Effects of Proximal Fibular Osteotomy on the Knee and Ankle Joints: a Finite Element Analysis

Vliv vysoké osteotomie fibuly na kolenní a hlezenní kloub: analýza konečných prvků

O. K. UNAL[1], M. Z. DAGTAS[1], C. DEMIR[2], T. NAJAFOV[1], E. UGUTMEN[1]

[1] Department of Orthopedics and Traumatology, Maltepe University Faculty of Medicine, Istanbul, Turkey
[2] Department of Mechanical Engineering, Yildiz Technical University, Istanbul, Turkey

ABSTRACT

PURPOSE OF THE STUDY

In this study, our aim is to examine the effect of proximal fibular osteotomy on knee and ankle kinematics with finite element analysis method.

MATERIAL AND METHODS

One 62-year-old, female volunteer's radiologic images were used for creating lower limb model. Osteotomized model (OM) which was created according to definition of PFO and non-osteotomized model (NOM) were created. To obtain a stress distribution comparison between the two models, 350 N of axial force was applied to the femoral heads of the models.

RESULTS

After PFO, the average contact pressure decreased 26.1% at the medial tibial cartilage and increased 42.4% at the lateral tibial cartilage. The Von Mises stresses decreased 57.1% at the femoral cartilage and decreased 79.1% at tibial cartilage. The stress on the tibial cartilage increased 44.6%, and stress on the talar cartilage increased 7.1% at the ankle joint.

CONCLUSIONS

FEA revealed that main loading at the knee joint shifted from medial tibial cartilage to the lateral tibial cartilage after PFO. Additionally, the stresses on each cartilage were redistributed across a wider and more peripheral area. FEA also demonstrated that the Von Mises stresses of the tibial and talar cartilages of the ankle joint increased after PFO.

Key words: knee pain, osteoarthritis, osteotomy, finite element analysis, axial loadings.

INTRODUCTION

Gonarthrosis is osteoarthritis of the knee joint, which is the progressive chronic degeneration of the joint cartilage. The main symptom of gonarthrosis is knee pain, and it is correlated with the severity of the arthritis (3). Gonarthrosis treatment is focused on relieving the pain that may occur during daily activities for milder cases or at rest for severe cases. Treatment modalities for gonarthrosis vary from lifestyle modification to arthroplasty. For geriatric patients, joint replacement surgery is generally accepted as the primary treatment option, but for early onset, gonarthrosis treatment options are challenging. Because of the need for revision with arthroplasty, many osteotomy techniques have been described for younger patients. The most popular technique is high tibial osteotomy, which is widely accepted for achieving satisfactory long-term results in the treatment of medial osteoarthritis (18). Many disadvantages of this technique (e.g., lateral cortical breakage, fixation failure, device irritation, alignment failure) have prompted the further search for another osteotomy option.

Proximal fibular osteotomy (PFO) was described, performed, and presented for the first time by Yang et al. in 2015 (28). In the literature, there are many studies about this osteotomy technique. Most have highlighted that the patients' knee pain decreased dramatically after the procedure. In these studies, it is assumed that load bearing in the knee shifted from the medial plateau to the lateral plateau of tibia after surgery, and this phenomenon caused the pain relief (21, 26). However, these assumptions need to be proved objectively.

The finite element analysis (FEA) is generally used in engineering and it is the computerized simulation of any given physical phenomenon which is used to reduce the number of physical prototypes, experiments and optimize components in their design phase to develop better products (23). Additionally, it is an important tool for simulating musculoskeletal diseases, physiological boundary conditions, orthopedic procedures and implant designs (4).

In this study, we set out to investigate how PFO affects knee and ankle joint. For this purpose, we used FEA and the following hypothesis were tested:

1) after PFO, maximum and average pressures change at the medial and lateral chondral surface of the tibia,

2) chondral surface stresses are redistributed at the knee and ankle joint after PFO,

3) after PFO, load distribution on the knee joint is changed,

4) PFO leads to change in alignment of lower limb.

MATERIAL AND METHODS

Study design

This study is an in silico trial, which was conducted between February 2020 and May 2020. For this study, one healthy female volunteer was selected with simple randomization method among patients who admitted with mild gonarthrosis and met the including criteria. The including criteria were; being between 55–70 years old, not having any operation at the lower extremities, not having severe lower extremity deformity or any leg length disparity. The volunteer signed an informed consent form to be included in this study. The study was approved by the ethics committee of Maltepe University Faculty of Medicine (No:2020/900/20). The volunteer's right lower limb was used to create an in silico lower limb model.

Digital image acquisition

In this study, we decided to collect weight-bearing, full-length radiographs of the right lower limb to document the true alignment and to realign the limb after three-dimensional (3D) modelling. Using the x-ray, we also checked any bony deformations of the lower limb. The alignment of the lower limb was calculated, and the Q angle of the knee was measured as 2º of varus. The 3D geometry of the models developed in this study were obtained using a 64-slice spiral computerized tomography (CT; Toshiba Aqulion 64-slice spiral) and 1.5-T nuclear magnetic resonance imaging (MRI; Philips Intera 1.5T Eindhoven, Netherlands).The geometry of the bones was reconstructed from the CT, and the geometry of the soft tissues was reconstructed from the MRI images. We used two sets of MRIs to scan the knee and the ankle joints, and a single set of CT images was used to scan the right lower limb from the femoral head to the foot. The MRI scan of the knee and ankle joints included the area 5 cm proximal and 5 cm distal from the joint line. The slice thickness and interval of both the MRI and CT images were 1.0 mm in a 256 × 256-pixel resolution. Images from the MRI and CT were saved in the digital imaging and communications in medicine (DICOM) format.

Three-dimensional modelling

First, the DICOM data set of 450 axial plane CT images was imported into Mimics (software version 21.0, Materialise, Leuven, Belgium) to reconstruct the surface geometry of the femur, tibia, fibula, and talus. During the segmentation process, pixel values representing a radiodensity greater than 300 HU (Hounsfield Units) were assigned to the bone (20). Finally, the 3D bone models were created and saved in the *.mcs* (Mathcad image file type) file format.

After the segmentation of the bones, the DICOM datasets of the ankle and knee, which were consisted of 90 axial plane MRI images, were imported into Mimics to reconstruct the surface geometry of the medial meniscus, lateral meniscus, femoral cartilage, tibial cartilage, tibial ankle cartilage, and talar cartilage. In the MRI dataset, bone structures were eliminated according to reference radiodensity values. Based on the literature, pixel values between 165 HU and 300 HU were accepted as joint cartilage (20). The lateral and medial menisci were created by manual masking of these soft tissues on each coronal plane segment using the marking tool in the Mimics software. After the segmentation process, the 3D volumetric models of the bones and soft tissues of the lower extremity were created with 2º of varus alignment at the knee joint (Fig. 1). All models were imported into the 3 Matic Research software (version 13.0, Materialise, Leuven, Belgium). The cartilage and menisci were aligned to the knee and ankle joints. All bone, cartilage, and meniscus models were fixed for errors, remeshed, and saved. The contact and boundary surfaces for the bones, cartilage, and ligaments were determined. All models were saved in the STEP file format for the ANSYS software (Canonsburg, Pennsylvania, USA).

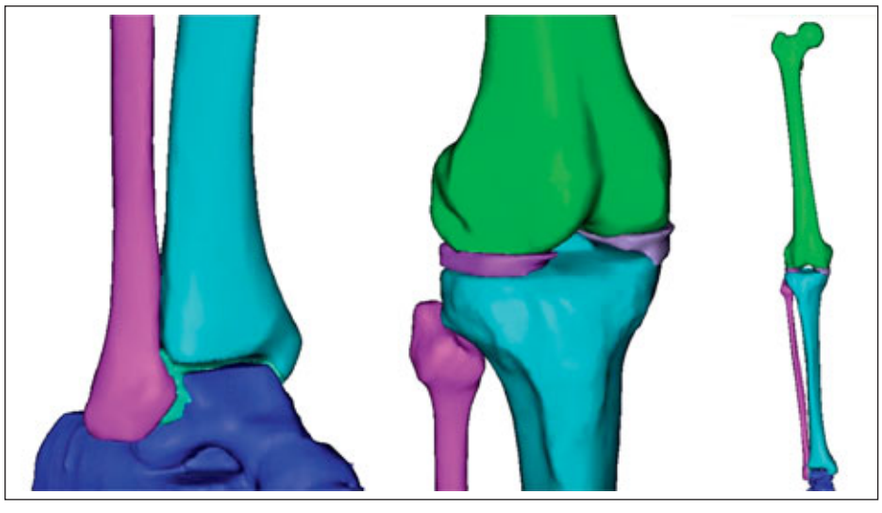

Fig. 1. Bones' images which were taken from CT images were segmented. After segmentation, soft tissue components were reconstructed by using MR images. Finally, 3D models of the bones and soft tissues of the (A) ankle, (B) knee and (C) lower limb were created.

Finite element modelling

All models were imported into the ANSYS software for FEA. Models were remeshed, and all bones, cartilage, and menisci were discretized into 10-node, tri-linear, tetrahedral elements. Tetrahedral elements were chosen over hexahedral elements due to their great flexibility in meshing complex, curved geometry. A refined mesh was used in

the articular cartilages and menisci. To mimic the anatomic model of the joint, the ligament system that provides the mechanical connection between the femur, tibia, fibula, and talus was created using spring elements in ANSYS.

Proximal fibular osteotomy modelling

We used two models of the lower extremity in this study. The first was the normal non-osteotomized model (NOM), and the second was the osteotomized model (OM). After the tetrahedral mesh was built in ANSYS for the OM model, two axial resection planes, which were between 6 cm and 10 cm distal from the proximal end of fibula, were created according to the definition of the PFO (28) (Fig. 2). The total numbers of elements and nodes for the NOM were 1,030,073 and 1, 522,751, respectively; for the OM, these values were 1,018,269 and 1,507,030, respectively. The element quality averages for the NOM and OM were 0.84556 and 0.84234, respectively.

Material properties

The ligament and cartilage material properties used in this study were determined according to the related literature. Various studies have assumed that the femur and tibia are hard bodies because they have high densities and high Young's modules compared to the cartilage and meniscus in the knee joint (16). On the other hand, most FEA studies have considered the entire bone structure of the knee joint as cortical bone (6, 30). Guess et al. developed a dynamic 3D anatomical knee joint model with enough computational competence for human motion simulation (6). In their study, the tibia was considered a rigid body, and the femur was assumed to be a linear elastic isotropic material with a Young's modulus of 17 GPa and a Poison's ratio of 0.2. Moreover, the cancellous bone was neglected, and the femur, tibia, and fibula were modeled as linear elastic isotropic material in the study conducted by Zheng et al. (30). In our study, the femur, tibia, fibula, and talus were assumed to be a linear elastic and isotropic material with a Young's Modulus of 17 GPa, a Poisson's ratio of 0.3, and a density of 1,600 kg/m³ (25). In the mathematical models of healthy human joints in the literature, cartilage is often represented as a single-phase, elastic material with homogeneous and isotropic properties (10). This value is valid when the cartilage is loaded for 1 to 5 seconds. During this time, the cartilage's response is elastic. Donzelli et al. proved that there are no significant changes in the cartilage contact response shortly after loading (5). After more than 1 minute, however, the response of the cartilage is dominated by the nonlinear, stress-relaxation-dependent viscoelastic properties (9). Hori and Mockros (10) also reported that the elastic modulus at the first second of loading for normal cartilage is in the range of 5.6 to 10.2 MPa, and for degenerative cartilage, it is in the range of 1.4 to 9.3 MPa. Poisson's ratio for normal and degenerative cartilage was also found to lie in the range of 0.42 to 0.49.

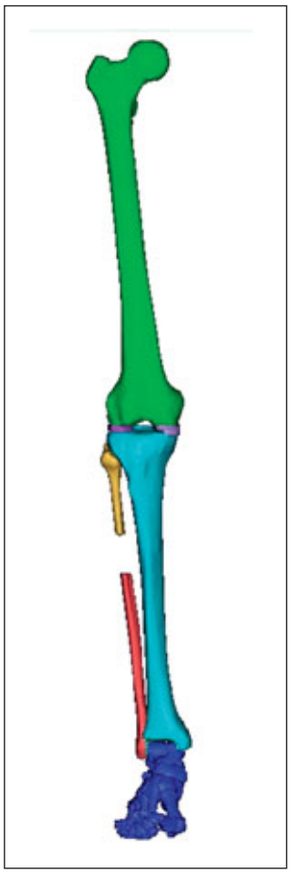

Fig. 2. Lower limb model with PFO was created according to literature.

In our study, the patient had grade 2 gonarthrosis. Thus, we assumed the elastic modulus of the knee cartilage was 1.4 MPa and that Poisson's ratio was 0.49. However, for the ankle joint, the cartilage elastic modulus accepted 1 MPa and a Poisson's ratio of 0.4 (29). In this study, the menisci were also specified as a single-phase linear isotropic and elastic material with the following average properties: an elastic modulus of 120 MPa, a Poisson's ratio of 0.475, and a density of 1,100 kg/m³ (4). To understand the process of loading and the stress distribution of the knee and ankle joints, we created all ligaments around the knee and ankle joint. Spring elements were used as knee and ankle ligaments in this study (Fig. 3A-D). All ligament names and stiffnesses that were created according to the literature are shown in Table 1.

Boundary conditions and loads

ANSYS was used to obtain approximate solutions to all static simulations in our study. Contact interfaces were modelled between the femoral cartilage, proximal tibia cartilage surfaces, and superior/inferior menisci surfaces in the knee as well as between the distal tibial cartilage and talar cartilage in the ankle. Attachment points were also generated between the femur and femoral cartilages, the tibia and proximal tibial cartilages, the talus and talar cartilages, and the tibia and distal tibial cartilages. All surfaces were modelled as frictionless (15). The "hard" contact model was used to define the surface interaction. This implies that no penetration of the nodes from one surface into the other surface was allowed. An augmented Lagrangian algorithm was used to simulate the contact between the femur cartilage and the superior surface of the menisci, the inferior surface of the menisci and the proximal tibia cartilage, and the distal tibial cartilage and the talar cartilage. The lubrication in the joint was assumed with frictionless behavior. During simulation, the talus bone was considered fixed in all degrees of freedom, and the tibia and femur were fixed in the coronal and sagittal degrees of freedom but free in the axial degree of freedom. The fibula translations were free in all degrees of freedom. Additionally, the rotations of the femur, tibia, and fibula were free in all degrees of freedom. Restriction of some anatomic components' movements which was obligatory to perform FEA, may influence the results. But it was thought to be negligible for

results of the study. Finally, a single axial force was applied to obtain the stress distribution at the articular cartilages of the knee and ankle for both NOM and OM, respectively, in this study. To obtain a stress distribution comparison between the two models, 350 N of axial force was applied to the femoral head.

RESULTS

The volunteer was 62-year-old woman with 70 kg of weight and 165 cm of height. In the NOM with mild varus and grade 2 gonarthrosis, the maximum contact pressure took place in the medial and posterior regions of the medial tibial cartilage, with a maximum of 2,300 KPa, and in the central region of the lateral tibial cartilage, with a maximum of 1,200 KPa. The maximum contact pressure values for the medial and lateral tibial cartilages were 386.4 KPa and 396.5 KPa, respectively in the OM (Fig. 4). Furthermore, the maximum contact pressures at the medial and lateral tibial cartilages decreased 83.2% and 66.9%, respectively after PFO. The average contact pressures for the medial and lateral tibial cartilages were 213.9 KPa and 120.3 KPa, respectively in NOM. The average contact pressures for the medial and lateral tibial cartilages were 157.9 KPa and 171.4 KPa, respectively in OM (Fig. 4). Additionally, the average contact pressure decreased 26.1% at the medial tibial cartilage and increased 42.4% at the lateral tibial cartilage after PFO.

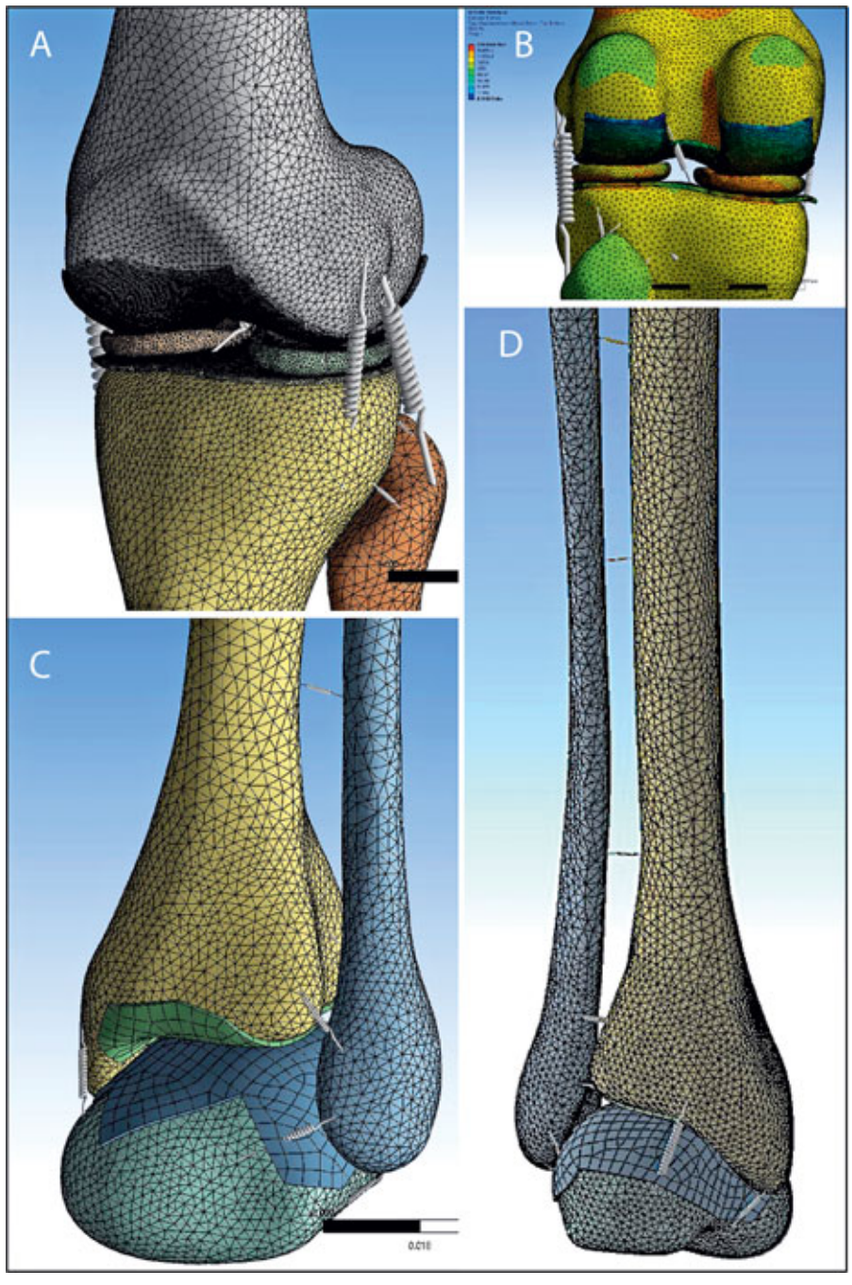

Fig. 3. Figures shows artificially created ligamentous structures of (A) anterior view of the knee joint, (B) posterior view of the knee joint, (C) anterior view of the ankle joint and (D) posterior view of the ankle joint.

The maximum Von Mises stress in the articular cartilages was obtained to assess the overall stress distribution. Our results for the knee with mild varus and grade 2 gonarthrosis revealed that the maximum Von Mises stresses in the femoral and tibial cartilages were equal to 320 KPa and 720 KPa, respectively. As the ankle joint cartilage stress distribution was also simulated in this study, the Von Mises stress in the ankle tibia and talar cartilages were equal to 103 KPa and 45 KPa, respectively in NOM. In the OM, the maximum Von Mises stresses in the femoral and tibial cartilages of the knee joint were equal to 137.51 KPa and 145.98 KPa, respectively. After PFO, 57.1% of the stress decreased at the femoral cartilage, and 79.1% decreased at tibial cartilage. The maximum Von Mises stresses for the tibial and talar ankle cartilage were equal to 149 KPa and 46 KPa, respectively. After PFO, the stress on the tibial cartilage increased by 44.6%, and stress on the talar cartilage increased by 7.1% at the ankle joint (Fig. 5). The Von Mises stresses were redistributed. For the medial tibial cartilage maximum, the Von Mises stress region moved from the central and posterior regions circumferentially to the anteromedial site of the cartilage. For

the lateral tibial cartilage, the maximum stress region also moved from its sharp central location circumferentially to the posterolateral site. The same explanation can be said for the femoral cartilage as well (Fig. 6A–D).

We calculated the average load for the medial and lateral tibial cartilages using the following equation (Equation 1);

$$F = P \times A, \qquad (3)$$

where F is the force, P is the pressure, and A is the area. As the areas of the medial and lateral tibia cartilages were 0.0013988 m² and 0.001268 m², respectively. The average loads for the medial and lateral tibial cartilages were 299.20 N and 152.54 N, respectively, in NOM. Thus, under a 350 N axial force, the lateral and medial tibial cartilage of the NOM carried 33.6% and 66.4% of the total load, respectively. In the OM, the load distributions for the medial and lateral tibial cartilages were calculated as 220.87 N and 217.33 N, respectively. Consequently, under a 350 N axial force, the lateral and medial tibial cartilage of the OM carried 49.6% and 50.4% of the total load, respectively.

Change of lower extremity alignment after PFO could not be evaluated due to boundary conditions of FEA.

DISCUSSION

In 2015, the PFO surgical technique was described (28), and since this time, many surgeons have performed this procedure for medial gonarthrosis. PFO has become more popular because of its small incision, short surgery

Table 1. Reference values of ligamentous structures (spring elements) of the knee and ankle joint

Knee and ankle ligaments (spring elements)		
Anatomic names	Stiffness (N/Mm)	Citations
ALL	20	(13)
FCL	33.5	(14)
PT	83.7	(14)
PFL	28.6	(14)
ApTFL	133	(17, 24)
ACL	1600	(8)
PpTFL	109	(2, 17, 24)
MCL deep	31.5	(27)
MCL superficial	31.5	(27)
Interosseous 1	100	(19)
Interosseous 2	100	(19)
Interosseous 3	100	(19)
Interosseous 4	100	(19)
AiTFL	78	(22)
AFTL	140	(22)
CFL	120	(22)
PiTFL	101	(1)
PFTL	160	(22)
Deltoid (anterior tibiotalar)	70	(22)
Deltoid (tibiocalcaneal + tibionavicular)	162	(22)
Deltoid (posterior tibiotalar)	80	(22)

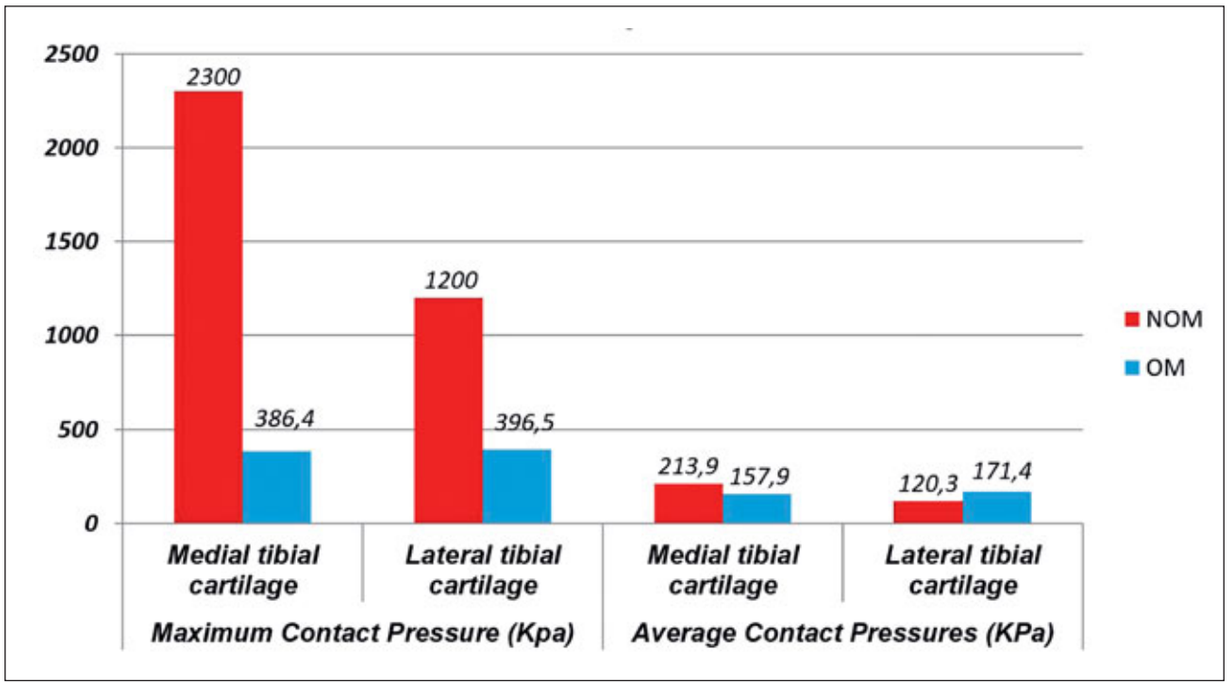

Fig. 4. Maximum contact pressure decreased at the medial and lateral tibial cartilage, but average contact pressures increased at the lateral tibial cartilage while it decreased at the medial tibial cartilage after PFO.

time, low complication rate, and low cost as well as the fact that it does not use any device and does not affect a TKA operation in the future (21). The main feature and advantage of PFO is the dramatic rapid pain relief immediately following the operation. There are many studies (21, 26) concerning PFO, and many authors agree that PFO is an effective treatment for pain relief in medial compartment knee osteoarthritis. Some theories have been suggested concerning the pain-relieving mechanism, but it has not been explained objectively. This study revealed that, although PFO is a minor surgical procedure, it has many effects on the knee and ankle joint. PFO effectively decreased the medial compartment stresses and increased the lateral compartment stresses in a mild varus and grade 2 gonarthrosis model. By this way, PFO provided homogeneous distribution of loading on medial and lateral tibial cartilage of the knee joint which was the major effect of PFO. More peripheral location of stresses on tibial and femoral cartilages of the knee joint was observed after PFO. Despite these advantages of PFO, surface stress elevation was observed at the ankle joint cartilages.

This study had a number of limitations. The main limitation of the study is that the musculature of the lower extremity was not included in the FEA. Some fibers of the flexor hallucis longus, peroneus longus, peroneus brevis, extensor digitorum longus, soleus, and tibialis posterior originate from the proximal fibula (12). These muscles, especially the peroneus longus and soleus, which pull the fibula distally, have direct effects on the proximal tibiofibular joint (PTFJ). After the partial resection of the proximal fibula, the PTFJ dynamics are likely to change, and this situation may contribute to reducing the pressure on the medial compartment of the knee. Second limitation of this study is that lower extremity alignment alteration was not evaluated by FEA. Shah et al. revealed that resection of the small part of the fibula caused a loss of lateral support of the fibula and a decrease in the lower extremity varus alignment (21). Additionally, there are some studies that have supported that the medial joint space shows widening with changing of lower extremity alignment after PFO (11). For example, Wang et al. reported that the medial joint space was increased, and the lower extremity alignment of the varus knee was corrected after PFO in radiographic measurements (26). However, alignment changes of lower limb and the widening of the medial joint space after PFO could not be evaluated in our study due to tibia and femur were fixed in the coronal degree of freedom.

The most widely accepted theory about pain relief after PFO is that PFO redistributes loading on the medial and lateral tibial plateaus. Especially for osteoporotic patients, the subchondral bone of the proximal tibial metaphysis loses trabecular support. The proximal tibiofibular joint helps the lateral condyle for transmitting weight, but the medial condyle has no such support. Asymmetric load transmission of the varus knee eventually creates more stress on the medial side, and arthritic changes occur with the degeneration of the articular cartilage. Therefore, varus deformity progresses with aging, and medial compartment osteoarthritis begins to form (21). After PFO, the lateral compartment loses support, and this situation leads to a shift in the stress from the

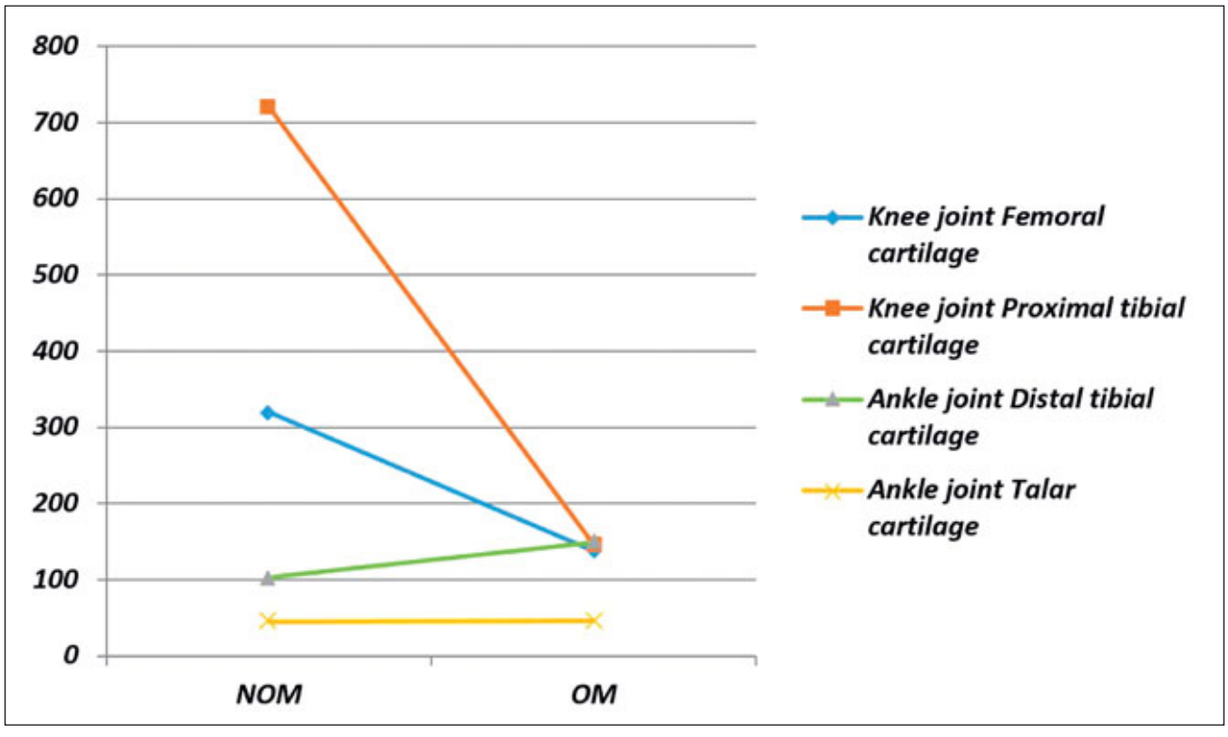

Fig. 5. Von Mises stresses of the knee joint cartilages dramatically decreased but stresses on ankle joint cartilages increased after PFO.

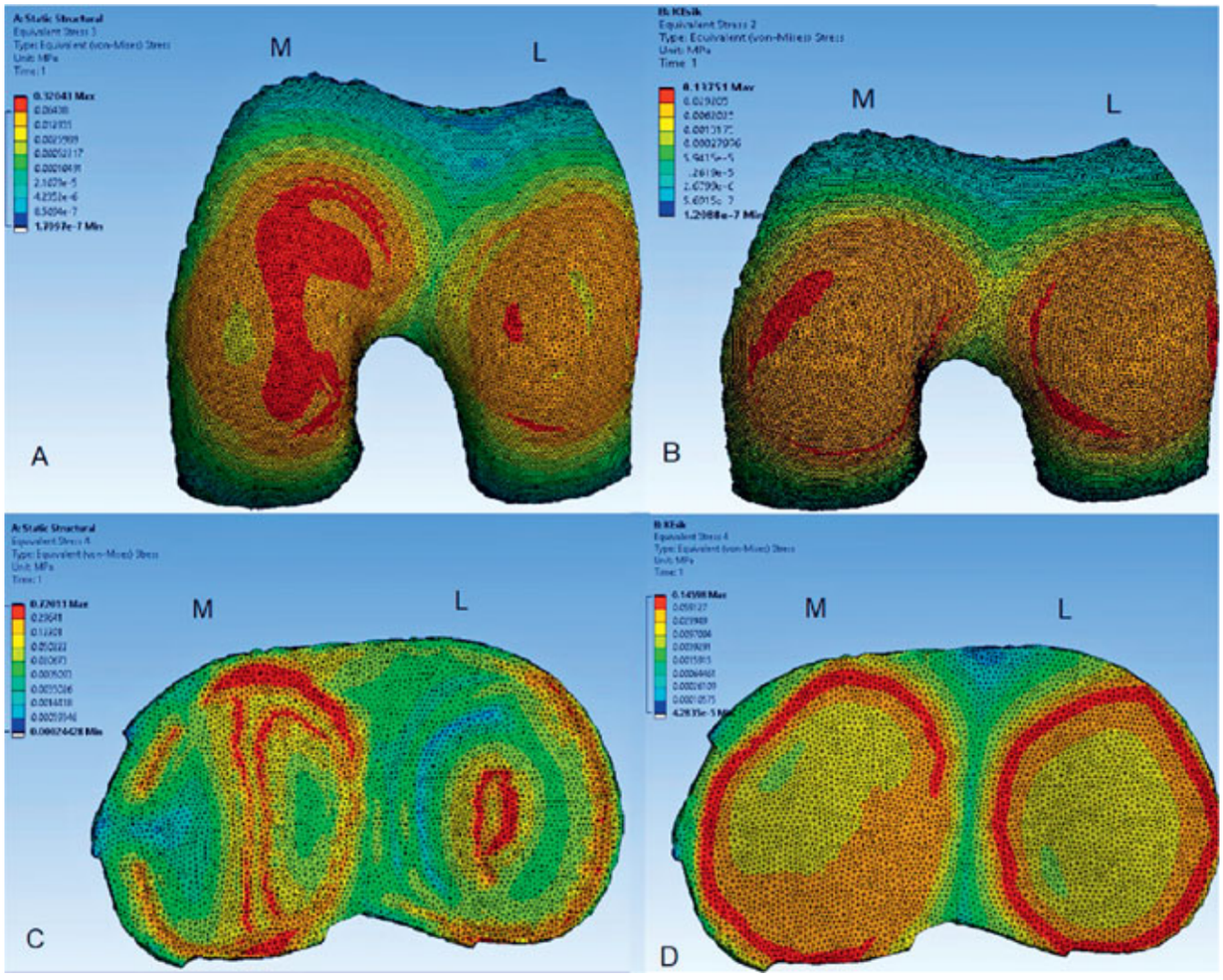

Fig. 6. Von Mises stresses concentrated intensely central part of femoral (A) and tibial (C) chondral surface at the NOM. However, high stress points moved to peripheral part of femoral (B) and tibial (D) cartilage of the knee joint after PFO.

medial to the lateral compartment of the knee, which results in pain alleviation (28). These studies all suggest that successful PFO outcomes are accompanied by the redistribution of the load after the removal of the proximal part of the fibula, which supports one-sixth of the body's weight. In our study, the maximum contact pressure decreased either the medial or lateral tibial cartilage more than 50%, indicating that the loading pressure distribution of the medial and lateral tibial cartilages changed after PFO. The loading pressure was distributed across a larger area instead of across a small part of the cartilage. The average contact pressure decreased at the medial tibial cartilage and increased at the lateral tibial cartilage. All these changes affected the Von Mises stress values of the tibial and femoral cartilages. After PFO, the Von Mises stresses of the femoral and tibial cartilages decreased prominently and redistributed across a wider area. Finally, before PFO the amount of the load that the medial tibial cartilage carried was two times more than the lateral tibial cartilage carried. However, after PFO, loading was redistributed more homogenously. These findings reveal that PFO caused lateral shifting of the loading pressure at the knee joint. These changes are the possible reasons for the dramatic pain relief after PFO.

To our knowledge, this is the first in silico study to analyze the ankle joint stress changes after PFO. While Guo et al. evaluated the ankle joint alignment changes after PFO (7), they noticed that the function of the ankle was improved but to a limited extent in radiographic results. Although the anatomical varus angulation was partly corrected, none of the patients underwent an anatomic valgus alignment postoperatively. Additionally, while preoperative hindfoot valgus angulation was significantly decreased, it still existed after the PFO procedure. In contrast, we evaluated the Von Mises stress changes after the PFO at the ankle joint. We identified that stress was increased at the tibial and talar cartilages of the ankle joint. These results could indicate that potential arthritic changes at the ankle joint will occur many years after PFO.

In conclusion, PFO has promising good results about knee gonarthrosis and may be the most effective option for the young patients with less complication rate. Many authors have shown satisfactory results concerning pain

relief and quality of life increases for patients after the PFO procedure. In our study, FEA has revealed objectively that PFO leads to changes at the knee and ankle joint. PFO caused a shift of the main loading pressure from the medial joint cartilage to the lateral joint cartilage of the tibia at the knee joint, and the stresses on each cartilage were redistributed across a wider and more peripheral area. The changes in knee kinematics could be the main reason for pain relief at the knee joint after PFO. FEA also demonstrated that the Von Mises stresses of the tibial and talar cartilages of the ankle joint increased after PFO. This stress increase may cause long-term arthritic changes in the ankle joint. More comprehensive FEAs are needed to reveal the effects of lower extremity musculature and lower extremity alignment changes after PFO.

Conflict of interest. *The authors report no conflicts of interest.*
Funding. *This study did not receive any specific grant from funding agencies in the public, commercial, or not-for-profit sectors.*

References

1. Beumer A, Van Hemert WL, Swierstra BA, Jasper LE, Belkoff SM. A biomechanical evaluation of the tibiofibular and tibiotalar ligaments of the ankle. Foot Ankle Int. 2003;24:426–429.
2. Caplan N, Kader DF. Biomechanical analysis of human ligament grafts used in knee-ligament repairs and reconstructions. In: Banaszkiewicz PA, Kader DF. Classic papers in orthopaedics. Springer, London Heidelberg New York Dordrecht, 2014, pp 145–148.
3. Dell'Isola A, Allan R, Smith SL, Marreiros SS, Steultjens M. Identification of clinical phenotypes in knee osteoarthritis: a systematic review of the literature. BMC Musculoskelet Disord. 2016;17:425.
4. Diffo Kaze A, Maas S, Arnoux PJ, Wolf C, Pape D. A finite element model of the lower limb during stance phase of gait cycle including the muscle forces. Biomed Eng Online. 2017;16:138.
5. Donzelli PS, Spilker RL, Ateshian GA, Mow VC. Contact analysis of biphasic transversely isotropic cartilage layers and correlations with tissue failure. J Biomech. 1999;32:1037–1047.
6. Guess TM, Thiagarajan G, Kia M, Mishra M. A subject specific multibody model of the knee with menisci. Med Eng Phys. 2010;32:505–515.
7. Guo J, Zhang L, Qin D, Chen W, Dong W, Hou Z, Zhang Y. Changes in ankle joint alignment after proximal fibular osteotomy. PLoS One. 2019;14:e0214002.
8. Haut Donahue TL, Hull M, Rashid MM, Jacobs CR. A finite element model of the human knee joint for the study of tibiofemoral contact. J Biomech Eng. 2002;124:273–280.
9. Hayes W, Mockros L. Viscoelastic properties of human articular cartilage. J Appl Physiol. 1971;31:562–568.
10. Hori RY, Mockros L. Indentation tests of human articular cartilage. J Biomech. 1976;9:259–268.
11. Jaheer HS, Shetty AA, Choi NY, Kim K-W, Thirumal SV, Song JS, Kim KS, Chun YS, Kim SJ. Preliminary results of high fibular osteotomy (HFO) and cartilage regeneration procedure for medial compartment osteoarthritis of knee with varus deformity. Regen Ther. 2019;10:112–117.
12. Kendall FP, Mccreary EK, Provance PG, Rodgers M, Romani WA. Muscles: testing and function with posture and pain. 5th ed., Wolters Kluwer Health, Philadelphia PA, 2005, pp 212–213.
13. Kennedy MI, Claes S, Fuso FaF, Williams BT, Goldsmith MT, Turnbull TL, Wijdicks CA, LaPrade RF. The anterolateral ligament: an anatomic, radiographic, and biomechanical analysis. Am J Sports Med. 2015;43:1606–1615.
14. LaPrade RF, Bollom TS, Wentorf FA, Wills NJ, Meister K. Mechanical properties of the posterolateral structures of the knee. Am J Sports Med. 2005;33:1386–1391.
15. Li G, Gil J, Kanamori A, Woo SL. A validated three-dimensional computational model of a human knee joint. J Biomech Eng. 1999;121:657–662.
16. Łuczkiewicz P, Daszkiewicz K, Chróścielewski J, Witkowski W, Winklewski PJ. The influence of articular cartilage thickness reduction on meniscus biomechanics. PLoS One. 2016;11:e0167733.
17. Marchetti DC, Moatshe G, Phelps BM, Dahl KD, Ferrari MB, Chahla J, Turnbull TL, LaPrade RF. The proximal tibiofibular joint: A biomechanical analysis of the anterior and posterior ligamentous complexes. Am J Sports Med. 2017;45:1888–1892.
18. Pannell WC, Heidari KS, Mayer EN, Zimmerman K, Heckmann N, Mcknight B, Hill JR, Vangsness CT, Hatch GF, Weber AE. High tibial osteotomy survivorship: a population-based study. Orthop J Sports Med. 2019;7:2325967119890693.
19. Pfaeffle HJ, Tomaino MM, Grewal R, Xu J, Boardman ND, Woo SLY, et al. Tensile properties of the interosseous membrane of the human forearm. J Orthop Res. 1996;14:842–845.
20. Riza S, Marlinawati D, Fahmi MaM. COMSeg technique for MRI knee cartilage segmentation. Int Rev Appl Sci Eng. 2019;10:147–155.
21. Shah R, Paudel S, Kalawar R. Role of proximal fibular osteotomy in medial joint osteoarthritis of knee. Austin J Orthopade & Rheumatol. 2018;5:1071.
22. Siegler S, Block J, Schneck CD. The mechanical characteristics of the collateral ligaments of the human ankle joint. Foot Ankle. 1988;8:234–242.
23. Simscale. What is FEA | Finite Element Analysis? . FEA | Finite Element Analysis: Simscale. Https://www.simscale com, 2021.
24. Van Seymortier P, Ryckaert A, Verdonk P, Almqvist KF, Verdonk R. Traumatic proximal tibiofibular dislocation. Am J Sports Med. 2008;36:793–798.
25. Walke W, Paszenda Z, Kaczmarek M. Biomechanical analysis of tibia-double threaded screw fixation. Archives of Materials Science and Engineering. 2008;30:41–44.
26. Wang X, Wei L, Lv Z, Zhao B, Duan Z, Wu W, Zhang B, Wei X. Proximal fibular osteotomy: a new surgery for pain relief and improvement of joint function in patients with knee osteoarthritis. J Int Med Res. 2017;45:282–289.
27. Wilson WT, Deakin AH, Payne AP, Picard F, Wearing SC. Comparative analysis of the structural properties of the collateral ligaments of the human knee. J Orthop Sports Phys Ther. 2012;42:345–351.
28. Yang ZY, Chen W, Li CX, Wang J, Shao DC, Hou ZY, Gao SJ, Wang F, Li JD, Hao JD, Chen BC, Zhang YZ. Medial compartment decompression by fibular osteotomy to treat medial compartment knee osteoarthritis: a pilot study. Orthopedics. 2015;38:e1110–1114.
29. Yu J, Cheung JT-M, Fan Y, Zhang Y, Leung AK-L, Zhang M. Development of a finite element model of female foot for high-heeled shoe design. Clin Biomech. 2008;23:S31–S38.
30. Zheng KK, Chen JN, Scholes C, Li Q. Magnetic resonance imaging (MRI) based finite element modeling for analyzing the influence of material properties on menisci responses. Applied Mechanics and Materials. 2014;553:305–309.

Corresponding author:
Omer Kays Unal, MD, Asst. Prof.
Maltepe Universitesi Tip Fakultesi Hastanesi
Ortopedi ve Travmatoloji Anabilim Dali
Feyzullah Cad. No: 39
34843 Maltepe / Istanbul, Turkey
E-mail: omerkays@gmail.com